Research Article Vol. 31, No. 1 / 2 Jan 2023 / Optics Express 44
Optics EXPRESS

Bound modes in the continuum in integrated photonic $LiNbO_3$ waveguides: are they always beneficial?

JIŘÍ ČTYROKÝ,[1,*] JIŘÍ PETRÁČEK,[2,3] VLADIMÍR KUZMIAK,[1] AND IVAN RICHTER[4]

[1]Department of Fiber Lasers and Nonlinear Optics, CAS Institute of Photonics and Electronics, Chaberská 57, 18200 Prague, Czech Republic
[2]Institute of Physical Engineering, Faculty of Mechanical Engineering, Brno University of Technology, Technická 2896/2, 61669 Brno, Czech Republic
[3]Central European Institute of Technology, Brno University of Technology, Purkyňova 656/123, 61200 Brno, Czech Republic
[4]Department of Physical Electronics, Faculty of Nuclear Sciences and Physical Engineering, Czech Technical University in Prague, Břehová 7, 11519 Prague 1, Czech Republic
*ctyroky@ufe.cz

Abstract: We discuss several types of integrated photonic $LiNbO_3$ waveguides supporting propagation of modes which can be classified as bound states in the continuum (BICs). The key properties leading to the existence of BICs (or quasi-BICs) considered here are the material anisotropy, the waveguide birefringence, or the combination of both. Typical examples are titanium diffused and proton exchanged waveguides in bulk $LiNbO_3$ crystals and recently proposed dielectric-loaded waveguides on $LiNbO_3$ thin films. Proton exchanged waveguides in thin film $LiNbO_3$ are considered, too. These waveguide structures are discussed from the point of view of their benefit for applications, especially in electro-optic devices.

1. Introduction

The concept of bound states in the continuum (BIC) was introduced nearly 90 years ago in quantum physics by von Neumann and Wigner [1] as a theoretical construction. Likewise to other concepts of theoretical and quantum physics represented by systems with *PT* symmetry [2], photonic crystals [3], or topological phases [4], BICs have found a number of interesting applications in photonics [5–10]. Photonic structures often offer possibilities to tailor the material and structural properties not available in quantum mechanics systems. Different kinds of BICs have been found in various photonic structures, and many of them have already been thoroughly investigated. Photonic BICs can be found in resonant structures – gratings, photonic crystals, metasurfaces, etc. Such BICs are represented with standing waves characterized by the quality factors approaching infinity. On the other hand, propagating BICs are represented with confined guided modes with suppressed coupling to the continuum of radiation modes into which they are embedded. The coupling can be suppressed, e.g., by destructive interference of two or more radiation channels due to particular device symmetry, or by polarization properties. In the case that the coupling is not completely suppressed, the modes propagate with nonzero radiation loss and can then be considered as quasi-BICs (q-BICs). In the established guided-wave terminology, they belong to the class of leaky modes [11].

It is well known that planar waveguides (with the refractive index depending only on one–transverse–coordinate) support pure TE and TM modes, while modes of integrated-optic channel waveguides (with refractive index depending on both transverse coordinates) are generally hybrid, with all electric and magnetic field components nonzero. However, they are often called

#477228 https://doi.org/10.1364/OE.477228
Journal © 2023 Received 3 Oct 2022; revised 13 Nov 2022; accepted 26 Nov 2022; published 19 Dec 2022

Optics EXPRESS

quasi-TE and quasi-TM, according to the orientation of their dominant transverse electric field component. In the following, the prefix quasi- will be omitted for brevity.

We start with revisiting one of the most traditional classes of integrated-optic waveguides–the planar and channel waveguides fabricated in the bulk $LiNbO_3$ single crystal substrate either by titanium diffusion [12] or by (annealed) proton exchange (PE) [13]. Although these waveguides have been widely employed in commercial devices such as fast electro-optic modulators already for decades, to our best knowledge, the fact that their extraordinary modes belong to the class of q-BICs has not been recognized yet. In the following, we explain in detail the physical reasons for such a classification.

Ti:$LiNbO_3$ and PE $LiNbO_3$ devices cannot be miniaturized due to their low refractive index contrast. This disadvantage can be overcome by using the lithium niobate on insulator (LNOI) configuration [14], which was inspired by the widely used high-contrast silicon on insulator (SOI) platform. In both these types of waveguide structures, the thin layer of silicon or lithium niobate represents a planar optical waveguide with high waveguide birefringence, which is in the case of $LiNbO_3$ combined with its natural anisotropy. For lateral confinement of light in these waveguides, ridge (fully etched down to the SiO_2 layer) or rib (partially etched) geometry is used. Whereas all modes of properly designed ridge waveguides are in theory perfectly guided, TM modes of shallow-etched rib waveguides may be lossy due to their coupling to the TE-polarized modes of the residual planar waveguide [15–21]. Radiation losses of these waveguides strongly depend on their width, and they vanish for some specific widths (often called "magic widths"). Modes of this type can be thus considered as BICs [19].

Low etching rate and anisotropy of the $LiNbO_3$ crystal renders the fabrication of channel (rib or ridge) LNOI waveguides difficult. In order to avoid this problem, a dielectric-loaded LNOI waveguides have been proposed, fabricated and tested [14]. Various materials as Si_3N_4, Ta_2O_5, TiO_2, or chalcogenide glass have been used. Optimized low-index polymer loaded Z-cut LNOI waveguides have been recently shown to support low-loss BIC TM modes [22]. Channel LNOI waveguides can be also created without etching by using proton exchange [23].

In Section 3 we critically asses the benefits which BIC modes supported by the polymer-loaded LNOI waveguides bring for integrated photonic devices, with respect to their non-BIC counterparts. We show that the standard non-BIC modes may be more advantageous not only because the design of the devices need not to follow the limitation to particular "magic widths" of the waveguides supporting the low-loss BICs, but their implementation can also substantially enhance the electro-optic efficiency of the devices since they allow to utilize the largest electro-optic coefficient of the $LiNbO_3$ crystal.

In Section 4 we show—also for the first time to our knowledge—that Z-cut LNOI waveguides fabricated by proton exchange support very low-loss q-BICs modes for arbitrary waveguide widths, while X-cut PE LNOI waveguides support standard (non-BIC) lossless modes only for directions of propagation under the large enough angles from the optic axis.

Hereafter, the notation X,Y,Z relates to the $LiNbO_3$ crystal axes, while the cartesian coordinates x,y,z are used to denote the lateral, vertical and longitudinal directions of the waveguide.

2. Titanium-diffused and proton-exchanged $LiNbO_3$ waveguides

Lithium niobate is a negative uniaxial crystal with the birefringence of about $n_{os} - n_{es} \approx 0.07$ (n_{os} and n_{es} being the ordinary and extraordinary refractive indices of the $LiNbO_3$ substrate) at the wavelength of 1.55 μm [24]. Titanium diffusion into the whole surface of the lithium niobate plate results in a planar (1D) waveguide. Channel (2D) waveguides are created by diffusion from the titanium stripe of the finite width. Resulting graded 1D or 2D refractive-index profiles are generally slightly different for extraordinary and ordinary polarizations [25,26], but both are typically lower than the natural crystal birefringence. In practical waveguides, the maximum variations of both indices at the waveguide surface are typically close to 0.01. The

Optics EXPRESS

waveguides are thus weakly guiding, with the dominant electric field components of their modes perpendicular to the waveguide plane for TM modes and parallel to the waveguide plane for TE modes. The effective refractive indices of extraordinary polarized waveguide modes are lower than the ordinary refractive index of the bulk crystal, and are thus necessarily embedded into the continuum of ordinary polarized radiation modes, with the potential to form BICs or q-BICs. Both planar and channel waveguides are commonly fabricated on the crystal Z-cut, for which the optic axis is perpendicular to the crystal surface, or on the X-cut, where the optic axis lies in the waveguide plane. The BICs or q-BICs can be found only among TM modes of the waveguides on the Z-cut and among TE modes of the waveguides on the X-cut. Whereas the direction of propagation does not play an important role in the Z-cut waveguides because of crystal symmetry, it is not the case for the X-cut waveguides, in which the effective refractive indices depend on the angle of the propagation direction with respect to the optic axis.

Figure 1 presents the graphs of the profiles with both ordinary and extraordinary refractive indices with indicated effective refractive indices of TE and TM guided modes propagating in the Y-direction in a *planar* (1D) X-cut waveguides at the wavelength of 1550 nm.

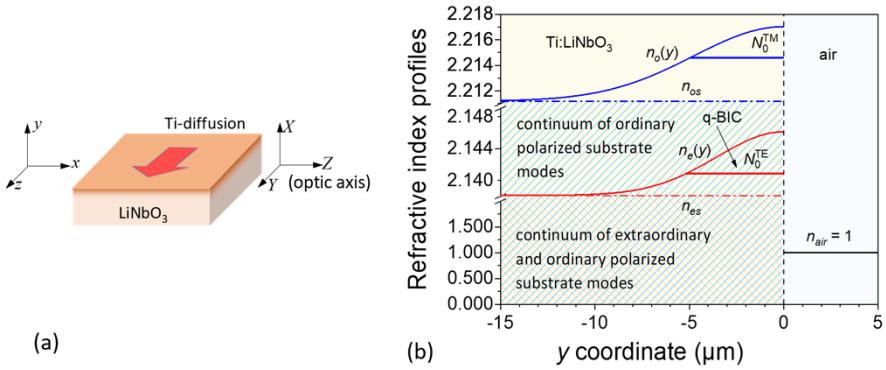

Fig. 1. a) Sketch of an X-cut Y-propagating planar Ti:$LiNbO_3$ waveguide with marked waveguide coordinates (x,y,z) and crystal axes (X,Y,Z); red arrow indicates the direction of light propagation. b) Refractive index profiles of the waveguide; n_{os} = 2.21122 and n_{es} = 2.13806 are the ordinary and extraordinary refractive indices of the substrate, N_0^{TM} and N_0^{TE} are the effective refractive indices of guided modes. The continua of substrate radiation modes with ordinary and extraordinary polarizations are marked by hatched areas.

Due to the $LiNbO_3$ crystal birefringence, the effective refractive index N_0^{TE} of the TE_0 mode is lower than the ordinary substrate refractive index n_{os}. While both electric field components of the TM_0 mode, E_y (vertical) and E_z (longitudinal), are perpendicular to the optic axis Z (coordinate axis x) and thus "see" the ordinary refractive index, the (only) E_x (lateral) component of the TE_0 mode of a planar waveguide "sees" the extraordinary refractive index. As a result, there is no coupling between the TE_0 mode field and the ordinary polarized substrate radiation continuum propagating in the same direction, in which the TE_0 mode is embedded. The TE_0 mode thus forms a pure, ideally lossless polarization protected BIC mode.

The TM modes of the Z-cut planar waveguides behave as lossless BICs, too. Their dominant electric field components are oriented along the Z axis and are thus controlled by the lower extraordinary refractive index. Since these modes cannot couple to the ordinary polarized substrate radiation continuum due to symmetry of the problem, they can be also considered as true lossless BICs. To our best knowledge, these facts have not been so far mentioned in the relevant literature about BICs.

Optics EXPRESS

Very similar situation occurs also in proton-exchanged and annealed (PE) $LiNbO_3$ waveguides [13,27]; the main difference is that only the extraordinary refractive index is increased while the ordinary index is decreased, so that only the extraordinary polarized wave can be guided. Guided modes of planar PE waveguides propagating perpendicularly to the optic axis are thus true lossless BICs since they do not couple to ordinary polarized substrate radiation continuum.

If the direction of propagation of a TE mode in X-cut Ti:$LiNbO_3$ or PE $LiNbO_3$ waveguides deviates by some angle from the Y-axis (i.e., from the direction perpendicular to the optic axis of the $LiNbO_3$ crystal), the modes become lossy due to the coupling to the ordinary polarized radiation continuum [28–30]. Their radiation losses then depend on the deviation angle. These modes, known for long as leaky (or semi-leaky) modes, can be classified—in the context of bound modes in the continuum—as q-BICs.

So far, we discussed the modes of planar (1D) waveguides. However, channel waveguides that confine the mode field in two dimensions perpendicular to the propagation direction are more important for applications. In principle, modes of channel waveguides are hybrid, i.e., all components of their electric and magnetic fields are generally nonzero. Therefore, some coupling of such modes with the substrate radiation continuum via the minority field components, resulting in the mode radiation loss, might be expected even for waveguides strictly perpendicular to the optic axis. However, we are not aware that this kind of radiation loss in channel Ti:$LiNbO_3$ or PE $LiNbO_3$ waveguides has already been discussed in literature, despite their broad commercial applications. In order to estimate the magnitude of such loss, we numerically calculated the complex effective indices of TM modes in a Z-cut Y-propagating Ti:$LiNbO_3$ waveguide, see Fig. 2(a), with the refractive index variations due to diffusion of the titanium stripe of the width w given by Eq. (1) [31] using the eigenmode solver in the Wave-optic module of the COMSOL Multiphysics [32]. Perfectly matched layers were applied to the boundaries of the calculation window to suppress unwanted reflections. The width w of the Ti stripe was varied from 1 to 10 μm, the diffusion width and depth were taken as $D_x = 4\mu m$, $D_y = 5\mu m$, respectively; the wavelength was 1.55 μm. These parameters approximately correspond to original titanium thickness of about 70 nm, the diffusion time 8 hours, and the diffusion temperature 1050°C.

$$\Delta n_e(x,y) = 0.005\left[\mathrm{erf}\left(\frac{w/2+x}{D_x}\right) + \mathrm{erf}\left(\frac{w/2-x}{D_x}\right)\right] e^{-\left(\frac{y}{D_y}\right)^2},$$
$$\Delta n_o(x,y) = (0.010834 \cdot \Delta n_e)^{0.55},\ y<0. \tag{1}$$

The calculated dependences of the real parts of the effective refractive indices of both the TE and TM modes on the titanium stripe width w are shown in Fig. 2(b). The TE modes are in theory lossless. For TM modes, very low radiation losses of the order of 10^{-3} dB/cm were calculated for arbitrary waveguide width w. These calculated losses are well below the typical measured propagating losses in real waveguides due to waveguide imperfections (surface scattering, absorption, etc.) [33]. Physical reasons why these modes can be classified as very low-loss q-BICs will be briefly discussed in Section 4.

In the X-cut channel waveguides, the radiation losses of the extraordinary polarized TE modes depend on the direction of propagation, likewise as in planar waveguides. Figure 3(a) shows the dependence of the (real parts of) the effective refractive indices of both the q-BIC TE_{00} and standard (non-BIC) TM_{00} modes on the propagation angle with respect to the Y crystal axis for the waveguide parameters given in (1) with $D_x = 5\mu m$, $D_y = 4\mu m$, and $w = 6$ μm, calculated using COMSOL Multiphysics. The wavelength considered is 1.55 μm. The upper left inset depicts the geometry of the problem, the bottom right one shows the polarization conversion which is known to occur for the propagation direction close to the optic axis [27–30]. Figure 3(b)) shows the q-BIC TE mode loss due to coupling with the ordinary polarized continuum of radiation modes. In the angular region of high loss (indicated by the dotted line in Fig. 3(b)), the results are not reliable due to very strong hybridization of the TE mode with radiation modes. The insets show

Optics EXPRESS

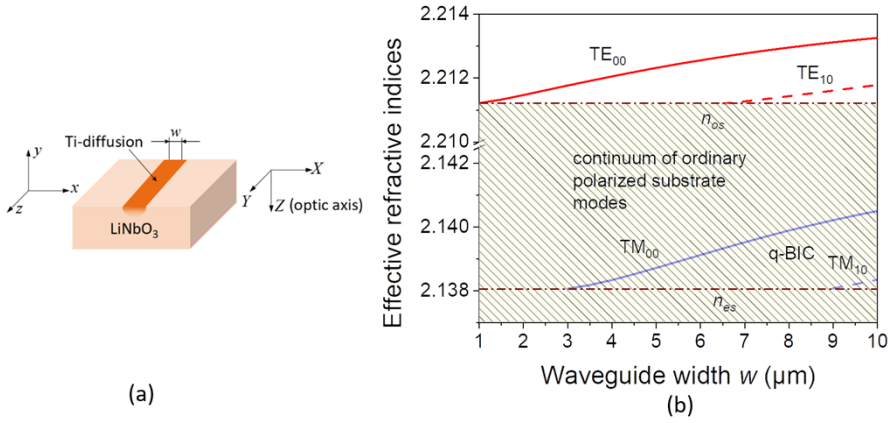

Fig. 2. a) Sketch of a Z-cut Y-propagating channel Ti:$LiNbO_3$ waveguide with the corresponding waveguide coordinates (x,y,z) and crystal axes (X,Y,Z). b) Dispersion curves of the waveguide.

the transversal mode field distributions for angles $\vartheta = 0°$, 60°, and 70°. For large angles, the radiation into the substrate is clearly visible.

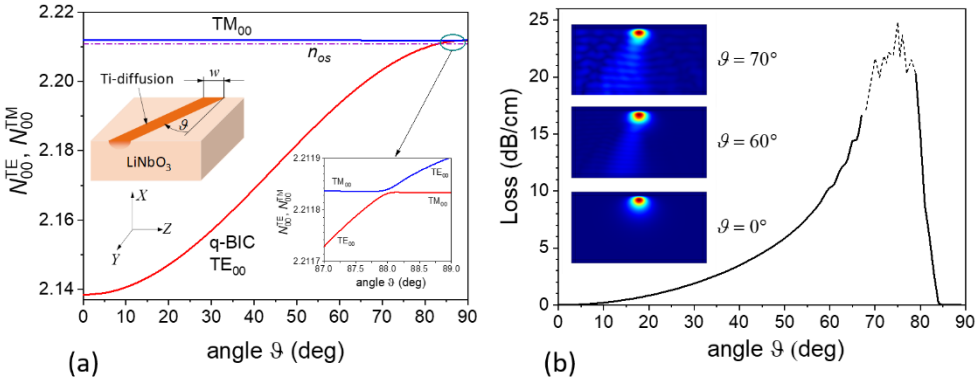

Fig. 3. X-cut Ti:$LiNbO_3$ channel waveguide propagating under an angle ϑ with respect to the Y-axis. a) Dispersion curves of TE_{00} and TM_{00} modes; the violet dash-dotted line indicates the ordinary refractive index of the substrate, the inset shows polarization conversion for $\vartheta \approx 88°$. b) Loss of the q-BIC TE_{00} mode; the results corresponding to the dotted part of the curve are unreliable due to numerical instabilities. The insets show mode field distributions for $\vartheta = 0°$, 60°, and 70°.

The TE mode of the waveguide directed along the Y axis can thus be classified as a very low-loss q-BIC.

Since the extraordinary refractive index profiles of practical proton exchanged channel waveguides are very similar to those of the Ti:$LiNbO_3$ waveguides and their losses are acceptably low [34] too, their modes can be also considered as q-BICs.

Most electro-optic $LiNbO_3$ waveguide devices are designed to utilize the strong electro-optic coefficient r_{33} which affects the extraordinary refractive index. It means that such devices operate with extraordinary polarized modes, i.e., BICs. Therefore, we can conclude that low-loss q-BICs are indispensable constituents of most integrated-optic $LiNbO_3$ devices of greatest practical importance like fast electro-optic modulators, polarization controllers, etc.

Optics EXPRESS

3. Polymer-loaded LNOI waveguides

Interesting integrated photonic devices using low-index loaded LNOI waveguides have been recently reported in [22,35,36]. In this design, a $LiNbO_3$ thin film of the thickness of a few hundreds of nanometers (240–400 nm) on the SiO_2 substrate is loaded by a polymer (ZEP520A electron resist) stripe of the height of about 500 nm and a variable width w, with air as the superstrate. Although the refractive index of the polymer (n_{poly} = 1.5429 at the wavelength of 1.55 μm) is substantially lower than both the extraordinary and ordinary refractive indices of the $LiNbO_3$ crystal, it is sufficient to laterally localize the optical field vertically confined by the $LiNbO_3$ slab and create thus a channel waveguide. The $LiNbO_3$ slab supports single planar TE_0 and TM_0 modes. Since the waveguide birefringence of the thin $LiNbO_3$ film is larger than the natural birefringence of the $LiNbO_3$ crystal, the effective refractive indices of TE modes are always higher than those of TM modes, for both X-cut and the Z-cut crystal films. In both cases, the effective indices of the TE_0 modes of the crystal slab waveguide propagating in arbitrary direction in the slab create the radiation continuum, into which the TM modes of the channel waveguides are embedded. The BIC or q-BIC modes can thus be found only among TM-polarized modes.

The loss mechanism of TM modes in dielectric-loaded channel waveguides is closely analogous to the well-known case of the TM modes in shallow etched rib waveguides [15–21]. For certain ("magic") widths of the channel waveguides, radiation losses of TM modes are strongly suppressed. Consequently, such modes can be considered as BICs.

To give an example, let us consider dielectric-loaded waveguides created on the Z-cut $LiNbO_3$ slab of the thickness of 400 nm with 500 nm thick loading polymer layer, as described in [22,35]. The dependences of (the real parts of) the effective indices of TE and TM modes and of the radiation losses of the TM modes of the channel waveguide on the width of the polymer stripe, calculated using COMSOL Multiphysics, are shown in Fig. 4. The waveguide cross-section is indicated in the inset of Fig. 4(b). As it is obvious from Fig. 4(a), the TE modes are regular lossless (non-BIC) modes, whereas the TM modes are embedded into the ordinary polarized continuum. The existence of "magic widths" for which the losses are minimized, is obvious from Fig. 4(b). The effective refractive indices of the corresponding BICs are indicated by points on the dispersion curves of TM modes in Fig. 4(a).

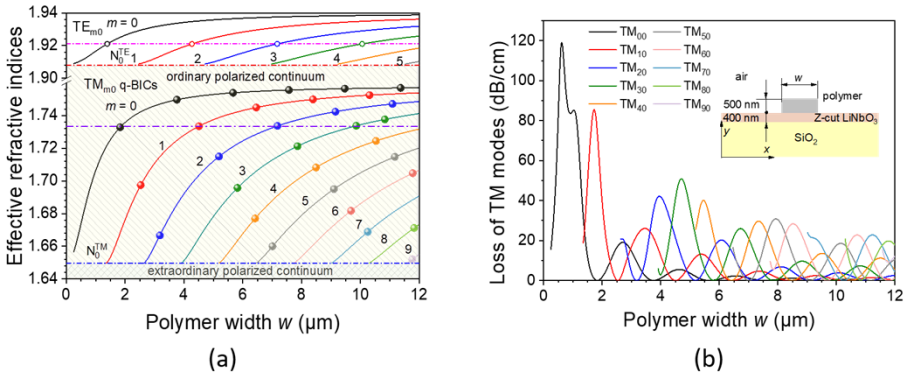

Fig. 4. a) Dispersion curves of the modes of the polymer loaded Z-cut LNOI channel waveguides. Dots indicate the positions of minimum radiation loss of TM_{m0} modes (BICs). b) Radiation losses of TM_{m0} modes in dependence of the polymer stripe width w. Inset shows the transversal cross-section of the waveguide.

Interestingly, the four lowest-order TM BIC modes exhibit essentially identical effective refractive indices close to 1.733 for the widths w of about 1.83, 4.51, 7.18, and 9.86 μm, as it is

Optics EXPRESS

indicated in Fig. 4(a) by dots connected with a violet dash-dot line. This fact has been utilized in [35] for the construction of the four-channel BIC TM mode de/multiplexer.

The electro-optic modulation of BIC TM modes using a pair of symmetric coplanar electrodes laterally placed along the channel waveguide has been also reported in [22] and [35]. However, as it was shown in [37], the modulation efficiency of such a modulator is extremely low. We note that a modified electrode configuration capable of exciting the electric field component parallel to the Z-axis, would enable significantly more efficient modulation.

Leaving aside the question of a long-term environmental stability of air-clad devices, the etchless fabrication of polymer-loaded LNOI waveguides is an indisputable advantage for potential applications. The advantage of the implementation of the BIC TM modes for the applications discussed above is less obvious, however. The TE modes of these waveguides are standard bound modes which propagate without radiation loss for any width w, for which they are supported. The choice of channel widths that lead to identical propagation constants of several TE lowest-order modes and thus enable the construction of the mode de/multiplexor analogous to that described in [35] is not restricted to "magic" widths as in the case of BIC TM modes. An example of such a choice is indicated in Fig. 4(a) by empty circles connected by the magenta short dot-dash line. Moreover, the electro-optic modulation of standard (non-BIC) TE modes with laterally placed coplanar electrodes [22] would be more efficient than the modulation of the BIC TM modes, for three following reasons. At first, the electric field of the TE mode is more strongly confined in the $LiNbO_3$ slab than that of the TM mode, as it is shown in Fig. 5. At second, the modulation of the TE polarized mode is mediated via the dominant electric field component, contrary to the case of the TM mode, and at third, the stronger electro-optic coefficient r_{33} is utilized.

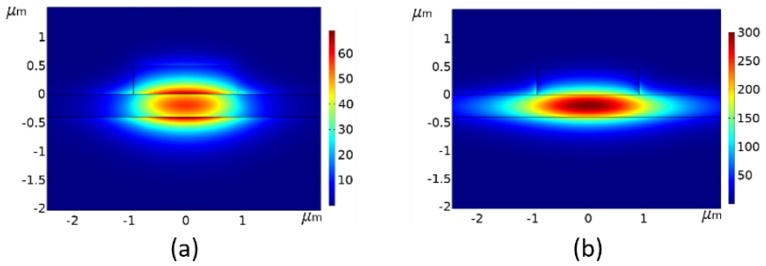

Fig. 5. Electric field distributions of the TM and TE modes in the polymer-loaded waveguide of the width $w = 1.83\mu m$ on the 400 nm thick $LiNbO_3$ slab. Polymer thickness is 500 nm, the wavelength is 1550 nm. a) TM mode, b) TE mode.

The application of the BIC TM mode in the polymer-loaded X-cut LNOI waveguide modulator has been recently described in [36]. The design makes use of the subwavelength grating waveguide close to the bandgap in order to increase the electro-optic modulation efficiency. Even in this case, the application of the non-BIC TE polarized mode, not restricted to any "magic" width, would significantly improve the efficiency of the electro-optic modulation. Although the dominant components of the electric field of the TE modes are extraordinary polarized, their effective refractive indices are higher than those of the TM modes due to the strong waveguide birefringence of the $LiNbO_3$ slab, at it is shown in Fig. 6. (The graph of TM mode radiation losses is not included for brevity.) Analogously to the previous case, the confinement of the electric field of the TE mode in the $LiNbO_3$ crystal slab is stronger, and the electro-optic modulation of this mode is mediated via the higher electro-optic coefficient r_{33}, instead of the three-times lower coefficient r_{13} involved in the modulation of the TM mode. Our COMSOL numerical simulations predict that the modulation of the TE mode requires about 7-times lower operation voltage for the same variation of the effective refractive index. (Note that for the TE polarization, the period of the subwavelength grating would have to be reduced from approximately 500 nm to

Optics EXPRESS

450 nm because of a higher effective refractive index of the TE mode.) The implementation of the BIC TM mode for the design of the modulator thus does not seem to bring any advantage over the design based on the (non-BIC) TE mode.

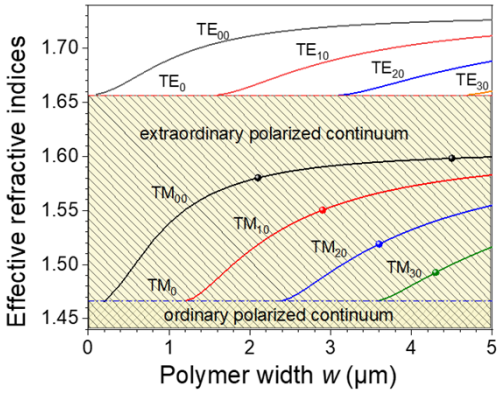

Fig. 6. Dispersion curves of the modes of the polymer loaded *X*-cut LNOI channel waveguides. The $LiNbO_3$ thickness is 240 nm, the polymer thickness is 500 nm, the wavelength is 1550 nm. Dots indicate the positions of TM BICs with minimum radiation loss.

As it has been recently shown [38], the BIC TM modes supported by the dielectric-loaded *Z*-cut LNOI waveguide can find potentially interesting applications also in the second harmonic generation (SHG). The phase matching can be ensured either between the TE_{00} mode at the pump wavelength and a properly chosen BIC TM_{m0} mode at the second harmonic wavelength or even between two q-BIC TM modes of different orders ([38] and the corresponding supporting information). For higher optical power load, silicon nitride can be used instead of the ZEP520A polymer. Thus, in contrast to the previous two examples, the implementation of BIC modes in this application seems to be indeed beneficial.

4. Proton-exchanged LNOI waveguides

The proton-exchanged (PE) LNOI waveguide [23] is another interesting waveguide configuration supporting the BIC mode. Its waveguide cross-section is schematically shown in Fig. 7(a). For the calculation of its eigenmodes, the variations of refractive indices due to proton exchange were approximated with the Gaussian profiles of refractive indices in the vertical (y) direction according to (2), with the surface values of 0.08 and –0.027, respectively, and with the diffusion depth $D_y = 1\,\mu$m. The ratio of about $-1/3$ between the ordinary and extraordinary surface index values corresponds to experimental results reported in [39]. The lateral diffusion was neglected for simplicity.

$$\Delta n_e(x,y) = \begin{cases} 0.08\exp[-(y^2, & |x| \le w/2, \\ 0, & |x| > w/2, \end{cases} \qquad \Delta n_o(x,y) = -0.027\Delta n_e(x,y). \tag{2}$$

The transverse distribution of the dominant electric field component E_y of the fundamental TM mode for the width $w = 2\mu$m calculated with COMSOL Multiphysics is shown in Fig. 7(b) (in arbitrary units), and the dependences of the effective refractive indices of guided modes on the PE section width w are shown in the graph in Fig. 7(c). The calculated radiation losses are graphically presented in Fig. 7(d).

Optics EXPRESS

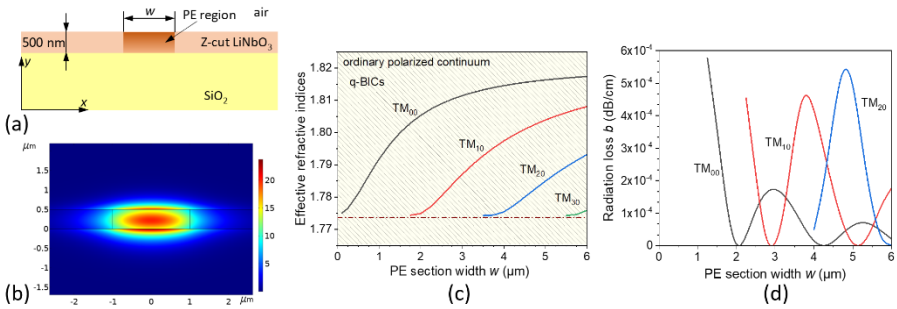

Fig. 7. a) Cross-section of the Z-cut proton-exchanged LNOI channel waveguide. b) Distribution of the dominant electric field component E_y of the TM_{00} mode for $w = 2\mu m$. c) Waveguide dispersion curves. d) Radiation losses of TM_{m0} modes in dependence of the PE section width w.

The effective refractive indices of the channel TM modes are substantially lower than the effective index of the (ordinary polarized) TE mode of the $LiNbO_3$ slab, $N_0^{TE} = 1.98070$ (not shown in Fig. 7(c)). It means that the PE channel TM modes are embedded into the continuum of the slab ordinary polarized TE_0 modes propagating in all directions, as it is indicated in Fig. 7(c). The loss curves in Fig. 7(d) exhibit behavior very similar to that of losses of polymer-loaded waveguide modes in Fig. 4(b), however the radiation loss values are extremely low for arbitrary waveguide width. This behavior can be explained by the following physical considerations. In case that the variation of the ordinary refractive index is neglected, the radiation continuum consists of TE_0 modes of the planar $SiO_2/LiNbO_3$/air waveguide propagating in any direction in the XY plane, the electric field components of which are perpendicular to the optic axis Z and are thus not affected by the variation of the extraordinary refractive index. These modes are thus the proper eigenmodes of the waveguiding structure (including the variation of the extraordinary refractive index), and as such they cannot be coupled to any other waveguide mode, including the TM_{m0} modes ($m = 1, 2, \ldots$) of the PE channel waveguide. It means that in such a structure, these modes are pure BICs. In real PE channel waveguides with nonzero variation of the ordinary refractive index, the TE_0 mode are no more the proper eigenmodes of the structure, therefore some coupling with the TM_{m0} modes is to be expected. Therefore, one can conclude that the TM_{m0} modes of the PE LNOI waveguides are very low-loss q-BICs.

In traditional Ti-diffused and PE waveguides in "bulk" $LiNbO_3$, the "ordinary polarized continuum" is more complex since the radiation modes propagate in a 3D space. Therefore, the coupling of TE-polarized channel waveguide modes with the continuum should be expected, which in fact has been confirmed by numerical simulations. The TE polarized modes of channel Ti:$LiNbO_3$ and PE $LiNbO_3$ waveguides are thus also q-BICs with low radiation loss.

The rotational symmetry of the Z-cut configuration ensures that the waveguide properties are independent of the direction in the XY plane (except the possible directional dependence of the lateral diffusion which was neglected here for simplicity).

Waveguides fabricated by the proton exchange into the X-cut $LiNbO_3$ slab support only standard (non-BIC) TE modes, due to the strong waveguide birefringence of the $LiNbO_3$ crystal slab. For completeness, the angular dependences of effective indices of the X-cut PE LNOI waveguide modes TE_{00} and TE_{10} are shown in Fig. 8.

In this case, the angularly dependent effective refractive index of the TE_0 mode of the planar LNOI waveguide propagating in parallel with the channel PE waveguide determines the upper boundary of the extraordinary polarized continuum and, as a result, it imposes restriction upon the angular region in which the TE_{m0} modes of the channel PE waveguide are supported. The

Optics EXPRESS

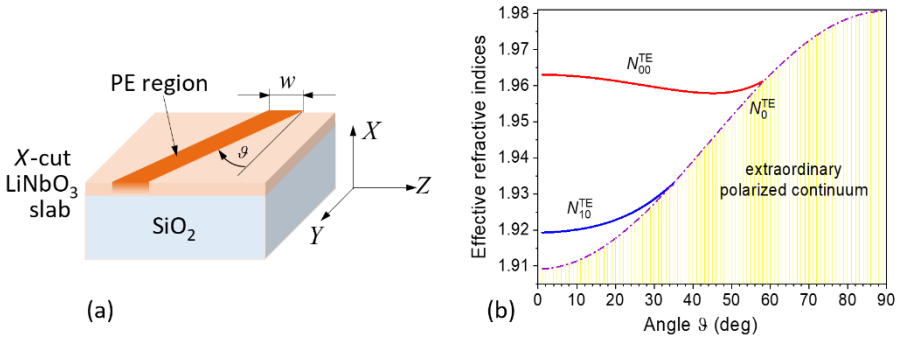

Fig. 8. a) Sketch of the X-cut PE LNOI waveguide directed under angle ϑ with respect to the Y-axis. b) Dispersion curves of the TE_{00} and TE_{10} modes of the PE waveguide with the refractive index profile given in Eq. (2). The $LiNbO_3$ slab thickness is 500 nm, the waveguide width is $w = 2\mu$m, the wavelength is 1.55 µm. The dash-dotted line indicates the angular dependence of the effective refractive index of the *planar* TE_0 mode of the $LiNbO_3$ slab. (The effective refractive index of the planar TM_0 mode, although ordinary polarized, is lower due to waveguide birefringence and is not shown in this figure.)

peculiar shape of the dispersion curve of the TE_{00} mode is the consequence of the negative variation of the ordinary refractive index within the PE region.

The PE fabrication also represents the etchless technology. The main challenge for successful technical applications of these unique single-polarization waveguides is to reduce the unwanted scattering loss while preserving high electro-optic and nonlinear-optic coefficients and high enough refractive index variation required for a strong mode confinement.

5. Conclusion

The concept of bound states in the continuum, originally arising from quantum mechanics, has been recently introduced also into photonics. From a number of various photonic structures in which the bound states in the continuum can be found, we concentrated in our paper just on one particular class—photonic waveguides in a $LiNbO_3$ crystal—and discussed potential benefits which the waveguide BICs could bring to practical integrated photonic devices.

Without any doubt, by far the most used integrated photonic devices utilizing q-BICs—although yet not generally recognized as such—are electro-optic modulators and similar electro-optic devices based on Ti:$LiNbO_3$ and PE $LiNbO_3$ fabrication technologies. Strong electro-optic interaction takes place for extraordinary polarized modes (TE modes on X-cut and TM modes on Z-cut) and extraordinary oriented applied electric field. As a result of the negative birefringence of the $LiNbO_3$ crystal, these modes are embedded into the continuum of ordinary polarized radiation. The graded-index character of the waveguides together with their small refractive index contrast renders the coupling between the confined guided modes and the radiation continuum very low. Therefore, such modes can be considered as very low-loss q-BICs for arbitrary waveguide widths.

In a novel recently developed LNOI platform, two approaches to the transverse localization of modes have been mostly used: the uneasy etching of the ridge waveguides into the $LiNbO_3$ slab, and the etchless fabrication using the deposition of a dielectric loading stripe onto the $LiNbO_3$ slab.

BIC TM modes in etchless polymer-loaded LNOI waveguides have been recently used in the design of integrated optic devices. Although this design undoubtedly represents an interesting advancement, we have shown here that similar functionality but with significantly higher electro-optic efficiency could be reached using standard (non-BIC) TE modes, not constrained to

Optics EXPRESS

special waveguide "magic widths". The BIC modes in these waveguides may find more fruitful applications, e.g., in nonlinear photonic devices.

Finally, we have shown by physical considerations as well as by numerical simulations that waveguides made by proton exchange in *Z*-cut LNOI support very low-loss q-BIC TM modes for arbitrary waveguide widths and an arbitrary direction in the *XY* plane. On the other hand, modes of the *X*-cut PE LNOI waveguide are standard lossless (non-BIC) TE-polarized modes, supported only within a limited angular range from the *Y*-axis.

The potential implementations of modes of PE LNOI waveguides in real-life applications would require significant technological improvements, however.

Funding. Ministerstvo Školství, Mládeže a Tělovýchovy (CZ.02.1.01/0.0/0.0/16_019/0000778); Grantová Agentura České Republiky (1900062S).

Disclosures. The authors declare no conflicts of interest.

Data availability. Data underlying the results presented in this paper are not publicly available at this time but may be obtained from the authors upon reasonable request.

References

1. J. v. Neumann and E. P. Wigner, "Über merkwürdige diskrete Eigenwerte," Phys. Z. **30**, 465–467 (1929).
2. C. E. Rüter, K. G. Makris, R. E-Ganainy, D. N. Christoulides, M. Segev, and D. Kip, "Observation of parity–time symmetry in optics," Nat. Phys. **6**(3), 192–195 (2010).
3. E. Yablonovitch, "Inhibited spontaneous emission in solid-state physics and electronics," Phys. Rev. Lett. **58**(20), 2059–2062 (1987).
4. L. Lu, J. D. Joannopoulos, and M. Soljačić, "Topological photonics," Nat. Photonics **8**(11), 821–829 (2014).
5. A. Kodigala, T. Lepetit, Q. Gu, B. Bahari, Y. Fainman, and B. Kante, "Lasing action from photonic bound states in continuum," Nature **541**(7636), 196–199 (2017).
6. L. Xu, K. Zangeneh Kamali, L. Huang, M. Rahmani, A. Smirnov, R. Camacho-Morales, Y. Ma, G. Zhang, M. Woolley, D. Neshev, and A. E. Miroshnichenko, "Dynamic Nonlinear Image Tuning through Magnetic Dipole Quasi-BIC Ultrathin Resonators," Adv. Sci. **6**(15), 1802119 (2019).
7. K. Koshelev, S. Kruk, E. Melik-Gaykazyan, J.-H. Choi, A. Bogdanov, H.-G. Park, and Y. Kivshar, "Subwavelength dielectric resonators for nonlinear nanophotonics," Science **367**(6475), 288–292 (2020).
8. V. Kravtsov, E. Khestanova, F. A. Benimetskiy, T. Ivanova, A. K. Samusev, I. S. Sinev, D. Pidgayko, A. M. Mozharov, I. S. Mukhin, M. S. Lozhkin, Y. V. Kapitonov, A. S. Brichkin, V. D. Kulakovskii, I. A. Shelykh, A. I. Tartakovskii, P. M. Walker, M. S. Skolnick, D. N. Krizhanovskii, and I. V. Iorsh, "Nonlinear polaritons in a monolayer semiconductor coupled to optical bound states in the continuum," Light: Sci. Appl. **9**(1), 56 (2020).
9. I. A. M. Al-Ani, K. As'Ham, L. Huang, A. E. Miroshnichenko, and H. T. Hattori, "Enhanced Strong Coupling of TMDC Monolayers by Bound State in the Continuum," Laser Photonics Rev. **15**(12), 2100240 (2021).
10. S. I. Azzam and A. V. Kildishev, "Photonic Bound States in the Continuum: From Basics to Applications," Adv. Opt. Mater. **9**(1), 2001469 (2021).
11. R. Sammut and A. W. Snyder, "Leaky modes on a dielectric waveguide: orthogonality and excitation," Appl. Opt. **15**(4), 1040–1044 (1976).
12. R. V. Schmidt and I. P. Kaminow, "Metal-diffused optical waveguides in $LiNbO_3$," Appl. Phys. Lett. **25**(8), 458–460 (1974).
13. J. L. Jackel, C. E. Rice, and J. J. Veselka, "Proton exchange for high-index waveguides in $LiNbO_3$," Appl. Phys. Lett. **41**(7), 607–608 (1982).
14. A. Boes, B. Corcoran, L. Chang, J. Bowers, and A. Mitchell, "Status and Potential of Lithium Niobate on Insulator (LNOI) for Photonic Integrated Circuits," Laser Photonics Rev. **12**(4), 1700256 (2018).
15. M. A. Webster, R. M. Pafchek, A. Mitchell, and T. L. Koch, "Width Dependence of Inherent TM-Mode Lateral Leakage Loss in Silicon-On-Insulator Ridge Waveguides," IEEE Photonics Tech. Lett. **19**(6), 429–431 (2007).
16. M. Koshiba, K. Kakihara, and K. Saitoh, "Reduced lateral leakage losses of TM-like modes in silicon-on-insulator ridge waveguides," Opt. Lett. **33**(17), 2008–2010 (2008).
17. T. G. Nguyen, R. S. Tummidi, T. L. Koch, and A. Mitchell, "Rigorous Modeling of Lateral Leakage Loss in SOI Thin-Ridge Waveguides and Couplers," IEEE Photonics Tech. Lett. **21**(7), 486–488 (2009).
18. A. P. Hope, T. G. Nguyen, W. Bogaerts, and A. Mitchell, "Experimental Demonstration of TM Lateral Leakage in a Standard SOI Photonics Platform," in *11th IEEE International Conference on Group IV Photonics (GFP)*, IEEE International Conference on Group IV Photonics, Paris, France, Aug. 27-29 (2014),
19. T. G. Nguyen, A. Boes, and A. Mitchell, "Lateral Leakage in Silicon Photonics: Theory, Applications, and Future Directions," IEEE J. Select. Topics Quantum Electron. **26**(2), 1–13 (2020).
20. S. T. Peng and A. A. Oliner, "Guidance and leakage properties of a class of open dielectric wave-guides .1. Mathematical formulations," IEEE Trans. Microwave Theory Tech. **29**(9), 843–855 (1981).
21. A. A. Oliner, S. T. Peng, T. I. Hsu, and A. Sanchez, "Guidance and leakage properties of a class of open dielectric wave-guides: New physical effects," IEEE Trans. Microwave Theory Tech. **29**(9), 855–869 (1981).

Optics EXPRESS

22. Z. J. Yu, X. Xi, J. W. Ma, H. K. Tsang, C. L. Zou, and X. K. Sun, "Photonic integrated circuits with bound states in the continuum," Optica **6**(10), 1342–1348 (2019).
23. L. Cai, S. L. H. Han, and H. Hu, "Waveguides in single-crystal lithium niobate thin film by proton exchange," Opt. Express **23**(2), 1240–1248 (2015).
24. U. Schlarb and K. Betzler, "Refractive indices of lithium niobate as a function of temperature, wavelength, and composition: A generalized fit," Phys. Rev. B **48**(21), 15613–15620 (1993).
25. M. Fukuma, J. Noda, and H. Iwasaki, "Optical properties in titanium-diffused $LiNbO_3$ strip waveguides," J. Appl. Phys. **49**(7), 3693–3698 (1978).
26. M. Minakata, S. Saito, M. Shibata, and S. Miyazawa, "Precise determination of refractive index changes in Ti-diffused $LiNbO_3$ optical waveguides," J. Appl. Phys. **49**(9), 4677–4682 (1978).
27. J. Čtyroký, "Light propagation in proton exchanged $LiNbO_3$ waveguides," Opt. Commun. **5**, 16–19 (1984).
28. J. Čtyroký and M. Čada, "Guided and semi-leaky modes in anisotropic optical-waveguides of $LiNbO_3$ type," Opt. Commun. **27**(3), 353–357 (1978).
29. S. K. Sheem, W. K. Burns, and A. F. Milton, "Leaky-mode propagation in ti-diffused $LiNbO_3$ and $LiTaO_3$ waveguides," Opt. Lett. **3**(3), 76–78 (1978).
30. K. Yamanouchi, T. Kamiya, and K. Shibayama, "New leaky surface-waves in anisotropic metal-diffused optical-waveguides," IEEE Trans. Microwave Theory Tech. **26**(4), 298–305 (1978).
31. P. Ganguly, D. C. Sen, S. Datt, J. C. Biswas, and S. K. Lahiri, "Simulation of refractive index profiles for titanium indiffused lithium niobate channel waveguides," Fiber Integr. Opt. **15**(2), 135–147 (1996).
32. COMSOL Multiphysics® v. 6.0. www.comsol.com. COMSOL AB, Stockholm, Sweden.
33. R. Regener and W. Sohler, "Loss in Low-Finesse Ti:$LiNbO_3$ Optical Waveguide Resonators," Appl. Phys. B **36**(3), 143–147 (1985).
34. M. L. Bortz and M. M. Fejer, "Annealed proton-exchanged $LiNbO_3$ waveguides," Opt. Lett. **16**(23), 1844–1846 (1991).
35. Z. Yu, Y. Tong, H. K. Tsang, and X. Sun, "High-dimensional communication on etchless lithium niobate platform with photonic bound states in the continuum," Nat. Commun. **11**(1), 2602 (2020).
36. J. Zhang, B. Pan, W. Liu, D. Dai, and Y. Shi, "Ultra-compact electro-optic modulator based on etchless lithium niobate photonic crystal nanobeam cavity," Opt. Express **30**(12), 20839 (2022).
37. J. Čtyroký and J. Petráček, "Comment on "Photonic integrated circuits with bound states in the continuum"," Optica **9**(7), 681–682 (2022).
38. F. Ye, Y. Yu, X. Xi, and X. Sun, "Second-Harmonic Generation in Etchless Lithium Niobate Nanophotonic Waveguides with Bound States in the Continuum," Laser Photonics Rev. **16**(3), 2100429 (2022).
39. M. De Micheli, J. Botineau, S. Neveu, P. Sibillot, and D. Ostrowsky, "Independent control of index and profiles in proton-exchanged lithium niobate guides," Opt. Lett. **8**(2), 114–115 (1983).